A Semiconducting Organic Radical Cationic Host–Guest Complex

Albert C. Fahrenbach,[†,‡,⊥] Srinivasan Sampath,[†,‡,⊥] Dattatray J. Late,[§] Jonathan C. Barnes,[†,‡] Samuel L. Kleinman,[†] Nicholas Valley,[†] Karel J. Hartlieb,[†] Zhichang Liu,[†] Vinayak P. Dravid,[§,*] George C. Schatz,[†,*] Richard P. Van Duyne,[†,*] and J. Fraser Stoddart[†,‡,*]

[†]Department of Chemistry, Northwestern University, 2145 Sheridan Road, Evanston, Illinois 60208-3113, United States, [‡]NanoCentury Korea Advanced Institute of Science and Technology, Institute and Graduate School of Energy, Environment, Water, and Sustainability (World Class University), Korea Advanced Institute of Science and Technology, 373-1, Guseong Dong, Yuseong Gu, Daejeon 305-701, Republic of Korea, and [§]Department of Materials Science and Engineering, Northwestern University, 2220 Campus Drive, Evanston, Illinois 60208-3108, United States. [⊥]Equal contributions.

ABSTRACT

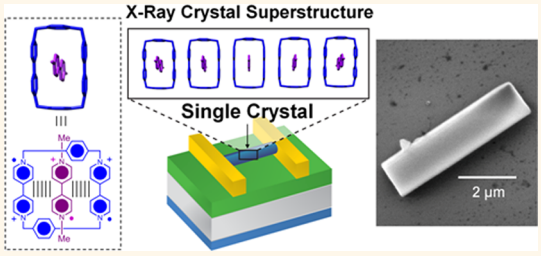

The self-assembly and solid-state semiconducting properties of single crystals of a trisradical tricationic complex composed of the diradical dicationic cyclobis(paraquat-*p*-phenylene) ($CBPQT^{2(\bullet+)}$) ring and methyl viologen radical cation ($MV^{\bullet+}$) are reported. An organic field effect transistor incorporating single crystals of the $CBPQT^{2(\bullet+)}\subset MV^{\bullet+}$ complex was constructed using lithographic techniques on a silicon substrate and shown to exhibit *p*-type semiconductivity with a mobility of 0.05 $cm^2\ V^{-1}\ s^{-1}$. The morphology of the crystals on the silicon substrate was characterized using scanning electron microscopy which revealed that the complexes self-assemble into "molecular wires" observable by the naked-eye as millimeter long crystalline needles. The nature of the recognition processes driving this self-assembly, radical–radical interactions between bipyridinium radical cations ($BIPY^{\bullet+}$), was further investigated by resonance Raman spectroscopy in conjunction with theoretical investigations of the vibrational modes, and was supported by X-ray structural analyses of the complex and its free components in both their radical cationic and dicationic redox states. These spectroscopic investigations demonstrate that the bond order of the $BIPY^{\bullet+}$ radical cationic units of host and guest components is not changed upon complexation, an observation which relates to its conductivity in the solid-state. We envision the modularity inherent in this kind of host–guest complexation could be harnessed to construct a library of custom-made electronic organic materials tailored to fit the specific needs of a given electronic application.

KEYWORDS: electrochemistry · molecular electronics · organic field effect transistors · quantum mechanics · Raman spectroscopy

Organic radicals are demonstrating[1] considerable promise as some of the active electronic building blocks for the construction of a variety of materials and devices, such as (i) molecular ferromagnets[2] containing two or more aligned spins, and (ii) nanoelectronic memory devices[3,4] which employ their reversible redox chemistries in order to switch between "on" and "off" states. They also are used for (iii) charge/energy storage in battery[5] and supercapacitor[6] applications and are (iv) implicit[7] as excitons in bulk-heterojunction organic solar cell technologies.

Historically, crystalline materials of continuously stacked organic π-radical cations have been known to exhibit[8−10] conducting behavior in a number of specific instances. Perhaps the best-known example of such an organic conducting crystal is one[11] composed of continuously π-stacked tetrathiafulvalene radical cations, $TTF^{\bullet+}$, along with segregated stacks of tetracyanohydroquinone radical anions, $TCNQ^{\bullet-}$. The driving force behind the recognition processes leading to the self-assembly of these continuous π-stacks is one of radical–radical interactions, also referred to[12,13] as "pimerization", which to a large extent involves spin pairing[14] of the free radicals, yielding a diamagnetic state. We and others have shown that these TTF radical cations can be enticed to dimerize[15−18] in solution by appealing to host–guest chemistry as well as within the molecular world of the mechanical bond in compounds containing mechanically interlocked components. Following on the heels of this initial discovery by Cowan and Perlstein[11] came the systematic study of many other radical cationic TTF derivatives in the solid-state, and their multifarious applications[19,20] in electronic and magnetic devices have been reported.

Using driving forces similar to those radical–radical interactions which lead TTF radical cations to dimerize in solution, radical cations of 1,1′-dialkyl-4,4′-bipyridinium ($BIPY^{\bullet+}$) derivatives have been known[21−25] since the 1960s to undergo dimerization in aqueous solutions. In 1990, Kochi[26] reported

*Address correspondence to stoddart@northwestern.edu.

Received for review August 6, 2012 and accepted October 3, 2012.

Published online October 18, 2012
10.1021/nn303553z

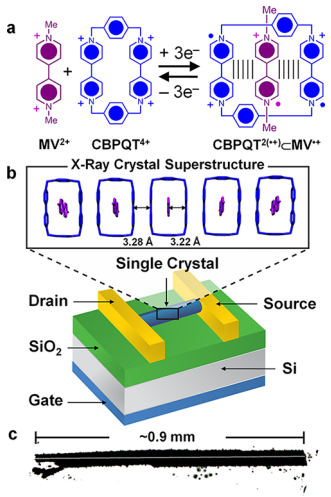

Figure 1. (a) The reversible redox active complexation of the $CBPQT^{4+}$ ring with MV^{2+} which occurs after reduction of their $BIPY^{2+}$ units to their radical cationic forms. The formation of the trisradical host–guest $CBPQT^{2(\bullet+)}\subset MV^{\bullet+}$ complex is driven by radical–radical interactions between its $BIPY^{\bullet+}$ components. (b) Schematic of the OFET constructed of single crystals of the $CBPQT^{2(\bullet+)}\subset MV^{\bullet+}$ complex. The inset shows the X-ray crystal superstructure of the trisradical complex (obtained from ref 28), revealing a continuous π-stack of $BIPY^{\bullet+}$ radical cations. The PF_6^- counterions and solvent molecules have been omitted for the sake of clarity. Note that the crystal structure was obtained at 100 K, while the OFET measurements were carried out at room temperature. (c) Optical image of a typical crystal of $CBPQT^{2(\bullet+)}\subset MV^{\bullet+}$ grown by slow-vapor diffusion of iPr$_2$O into a MeCN solution of the complex.

the solid-state structure of the methyl viologen radical cation, which, like $TTF^{\bullet+}$, also forms a continuous π-stack. He showed that the methyl viologen radical cation ($MV^{\bullet+}$) possesses conductivity when measured in the solid state as a bulk powder. Recently, we have described[27,28] a trisradical trication complex involving the entry of $MV^{\bullet+}$ inside the cavity of the diradical dicationic cyclobis(paraquat-*p*-phenylene) ($CBPQT^{2(\bullet+)}$) ring (Figure 1A). The formation of this host–guest complex occurs spontaneously ($K_a = 5.04 \times 10^4$, 298 K, MeCN) by radical–radical interactions, a process which is orders of magnitude stronger than the dimerization of $MV^{\bullet+}$ under the same conditions. This enhanced stability, which we exploit here in our design strategy for growing crystals to be used in device fabrication, is presumably a consequence of the precise preorganization of the $MV^{\bullet+}$ guest provided by the cavity of the $CBPQT^{2(\bullet+)}$ host. The single-crystal X-ray analysis of this trisradical cationic $CBPQT^{2(\bullet+)}\subset MV^{\bullet+}$ complex reveals[28] a continuous π-stack of radical cations in the solid state, interactions within which are responsible for the facile self-assembly into needle-like morphologies observable as single crystals on the micro- to millimeter scale (Figure 1C). Furthermore, we have shown that these radical–radical interactions can be employed[29] in the template-directed synthesis of mechanically interlocked molecules[30] (MIMs) and can be used in the design[31] of bi- and multistable MIMs that can be switched in both aqueous and organic solvent systems. Herein, we report the solid-state semiconductive properties of single crystals of the $CBPQT^{2(\bullet+)}\subset MV^{\bullet+}$ complex and their Raman spectroscopic behavior in both the solution and solid states. An in-depth analysis of the X-ray crystal structures is presented, which is supported by Raman spectroscopy, and takes into consideration the bond order of the $BIPY^{2+/\bullet+}$ subunits of the components in their free and complexed forms, comparing donor–acceptor to radical–radical interactions.

RESULTS AND DISCUSSION

Organic Field Effect Transistor Experiments. To assess the electronic conductivity of the $CBPQT^{2(\bullet+)}\subset MV^{\bullet+}$ complex in the solid state, we have fabricated an organic

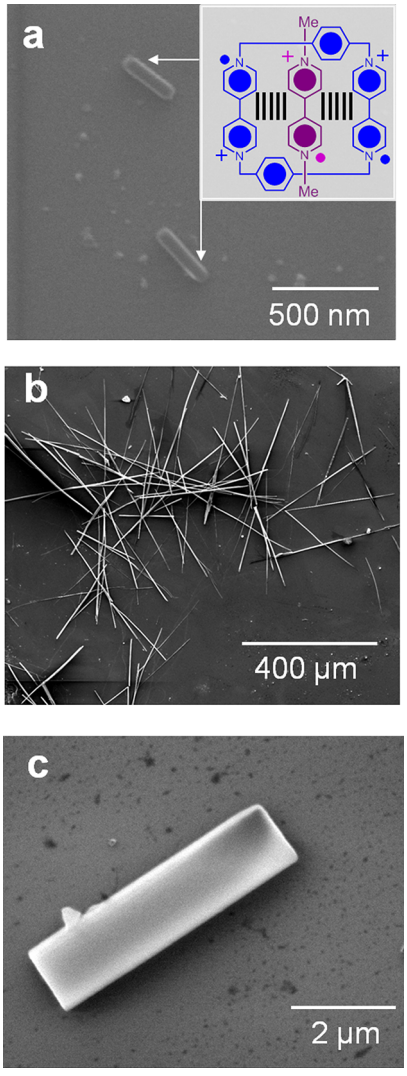

Figure 2. SEM images of single crystals of the $CBPQT^{2(\bullet+)}\subset MV^{\bullet+}$ complex obtained on a Si/SiO$_2$ substrate. Single crystals were grown directly on the surface by slow vapor diffusion of iPr$_2$O into a MeCN solution of $CBPQT^{2(\bullet+)}\subset MV^{\bullet+}$ layered on the silica wafer. Similar crystal morphologies were observed (a–c) in all cases, differing only in specific dimensions. The long axis of the crystals lie parallel to the π-stacking axis of the $BIPY^{\bullet+}$ units shown in Figure 1.

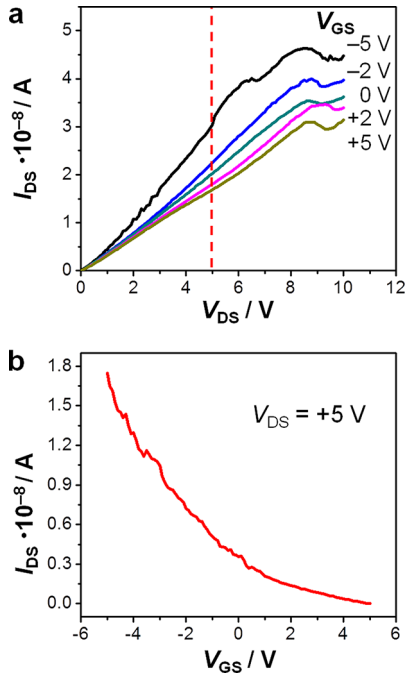

Figure 3. (a) The *I*−*V* curves as a function of V_{DS} recorded at varying gate voltages (V_{GS}, −5 to +5 V) obtained from the OFET constructed from single crystals of the CBPQT$^{2(\bullet+)}$⊂MV$^{\bullet+}$ complex employing lithographic techniques. (b) A plot of the magnitude of the current running through the crystal as a function of V_{GS} read at a constant drain-source potential (V_{DS}). The fact that the magnitude of the current decreases toward zero at increasingly positive values of V_{GS} is indicative of *p*-type semiconduction by these CBPQT$^{2(\bullet+)}$⊂MV$^{\bullet+}$ crystals.

field-effect transistor (OFET) device (Figure 1B) using single-crystal samples. Crystals of the CBPQT$^{2(\bullet+)}$⊂MV$^{\bullet+}$ complex were grown directly onto silicon wafers. Once in the solid state (Figure 1C), the BIPY$^{\bullet+}$ radical cationic components are resistant to oxidation by atmospheric O_2 and may be handled under ambient conditions thereafter for weeks.

We have used scanning electron microscopy (SEM) in order to characterize the surface morphology (Figure 2) of the single crystals of the CBPQT$^{2(\bullet+)}$⊂MV$^{\bullet+}$ complex on the silicon wafer substrate. The results mimic those which can be observed with the naked eye when growing crystals for single-crystal X-ray analysis, namely, that long needle-like crystals are observed also on the SiO_2/Si substrate surface. The long-axis of the crystals coincide with the *a*-axis of the unit cell, along which the CBPQT$^{2(\bullet+)}$⊂MV$^{\bullet+}$ complexes π-stack through radical−radical interactions. It is along this dimension we carried out our investigations of electric conductivity.

We have employed e-beam lithographic techniques to construct OFETs from single crystals of the CBPQT$^{2(\bullet+)}$⊂MV$^{\bullet+}$ complex grown on the degenerately doped SiO_2/Si substrates. Figure 3 shows the room temperature bottom-gate OFET characteristics of the CBPQT$^{2(\bullet+)}$⊂MV$^{\bullet+}$ complex as its single crystal. The output (Figure 3A) and transfer (Figure 3B) characteristics were measured by applying a V_{DS} to a pair of Ti/Au patterned source-drain electrodes and gate voltage V_{GS} to the back gate silicon substrate electrode. The OFET devices were annealed under an inert atmosphere at 150 °C in order to promote low contact resistance. The back gating characteristics of the devices are typical of a *p*-type channel conductance. After applying the V_{GS} sweeps repeatedly on an OFET device, we did not observe any significant variation while keeping I_{DS} constant, an excellent indication of the robustness[32] of the device. The field effect mobility (μ) of OFET devices was calculated[33] using eq 1:

$$\mu = [dI_{DS}/dV_{GS}] \times [L/W \times C_i V_{DS}] \quad (1)$$

where *L* is channel length (10 μm), *W* is channel width (40 μm), C_i (6.9×10^{-5} F/cm^2) is the gate capacitance between the channel and the silicon back gate per unit area which is given by $C_i = \varepsilon_0\ \varepsilon_r/d$, where ε_0 (3.9) and *d* (500 nm) are the dielectric constant and thickness of SiO_2, respectively. The field effect mobility was calculated to be ~0.05 cm^2 V^{-1} s^{-1}.

X-ray Structural Analyses. To obtain a deeper understanding of the radical−radical interactions in the solid state which give rise to the semiconducting behavior of the CBPQT$^{2(\bullet+)}$⊂MV$^{\bullet+}$ complex, we have carried out an in-depth analysis of the changes in bond lengths and torsional angles between radical and oxidized forms, for both free and complexed components (Figure 4) as measured from single-crystal X-ray structural data.

Our previous quantum mechanical and EPR investigations support[27] the hypothesis that only two of the

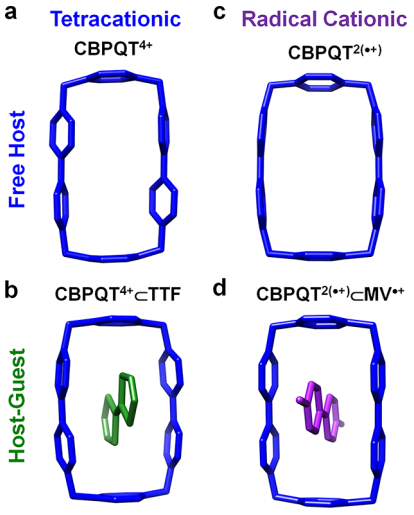

Figure 4. Solid-state structures determined by X-ray crystallography of the π-electron deficient tetracationic CBPQT^{4+} (a, ref 38), its CBPQT^{4+}⊂TTF complex (b, ref 39), the diradical dicationic CBPQT$^{2(\bullet+)}$ ring (c, ref 28) and its CBPQT$^{2(\bullet+)}$⊂MV$^{\bullet+}$ complex (d, ref 28). Note that the torsional angle of the BIPY^{2+} units decrease significantly upon complexation of CBPQT^{4+} with TTF. The change in the torsional angles for the BIPY$^{\bullet+}$ units upon complexation of CBPQT$^{2(\bullet+)}$ with MV$^{\bullet+}$ remain relatively unperturbed. In all cases, the PF_6^- counterions and solvent molecules have been omitted for the sake of clarity.

radicals of the trisradical complex are spin-paired (singlet) at any given instance in time, yielding a net paramagnetic (doublet) state. In their dicationic forms, $BIPY^{2+}$ units commonly adopt relatively large torsional angles (~35°) between their two pyridinium rings. These torsional angles are a consequence of free rotation about the central 4,4′-C−C bond which allows the two pyridinium rings to twist into a lower energy conformation. When the LUMO of $BIPY^{2+}$ becomes populated with electron density donated from the HOMO of π-electron-rich species, however, the central 4,4′-C−C bond takes on double-bond character. This situation happens as a consequence of the antibonding nature of the LUMO, which acts to shorten the length of some C−C bonds while elongating others in a manner that leads to an overall reduction of the bond order in the $BIPY^{2+}$ unit. The consequence of the 4,4′-C−C bond taking on double-bond character is that free rotation about this axis becomes hindered, and the two pyridinium units become more coplanar with each other, as indicated by the observation that their torsional angles tend toward 0° in these cases. These similar effects on the structure of the $BIPY^{2+/\bullet+}$ units for either donor−acceptor or radical−radical complexes points to the similarities[34,35] of the fundamental orbital interactions governing the recognition processes at play during these two seemingly different, although reciprocally related motifs.

First of all, let us consider the case[36−38] of the fully oxidized tetracationic $CBPQT^{4+}$ ring in the solid state. The length of the central 4,4′-C−C bond is 1.48 Å, while the torsional angle is 40°. Upon complexation[39] with the neutral π-electron-rich TTF, the torsional angle decreases to 9.8°, concomitant with changes in the C−C bonds lengths identified in Table 1. This change in the bond order brought about by donor−acceptor interactions is further expressed[40] in the molecular world in the case of a [2]catenane composed of the $CBPQT^{4+}$ ring mechanically interlocked with a macrocyclic polyether containing TTF and 1,5-dioxynaphthalene π-electron-rich units. For details of the structure, see reference 40. Quantum mechanical calculations performed[41,42] on both the free $CBPQT^{4+}$ host and the $CBPQT^{4+}\subset TTF$ complex support the hypothesis that a change in bond order occurs upon complexation, and that the LUMO is most likely localized to the $CBPQT^{4+}$ component while the HOMO is localized to TTF leading to inhibition of conductivity when expressed in the solid-state as mixed donor−acceptor stacks.

We now examine the changes in bond lengths on going from the fully oxidized $CBPQT^{4+}$ ring to its diradical dicationic $CBPQT^{2(\bullet+)}$ form. The torsional angle of the $BIPY^{\bullet+}$ radical cationic components of the ring decreases to 2.60°, and the length of the central 4,4′-C−C bond further decreases to 1.43 Å. These changes in geometry are a consequence of

TABLE 1. Bond Length and Torsional Data Obtained from Crystallographic Analysis of Free $BIPY^{2+/\bullet+}$ Units, When They Are Engaged in Donor−Acceptor Interactions with Electron-Rich Guests, and in Their Radical Cationic Forms[a]

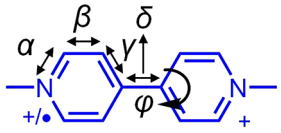

species	α (Å)	β (Å)	γ (Å)	δ (Å)	φ (deg)
$CBPQT^{4+}$[b]	1.34	1.38	1.39	1.48	40.0
$CBPQT^{4+}\subset TTF$[c]	1.33	1.37	1.39	1.48	9.75
[2]Catenane[d]	1.34	1.37	1.40	1.49	1.87
$CBPQT^{2(\bullet+)}$[e]	1.35	1.37	1.43	1.43	2.60
$MV^{\bullet+}$[f]	1.37	1.34	1.42	1.42	8.96
$CBPQT^{2(\bullet+)}\subset MV^{\bullet+}$[e]	1.37	1.35	1.43	1.43	0.38
	1.36	1.36	1.42	1.43	0.07

[a] The illustration in the caption defines the bond distances and torsional angle. All distances and angles correspond to the average value measured across the unit cell. The X-ray data shown is based on structures with PF_6^- counterions reported in the references. [b] Data from ref 38. [c] Data from ref 39. [d] Data from ref 40. [e] Data from ref 28. [f] Data from ref 26.

populating the antibonding orbital with the radical electron, a situation which causes an increase in the sp^2 character of the central bond. The solid-state structure of the methyl viologen radical cation ($MV^{\bullet+}$) reported by Kochi,[26] reveals a torsional angle of 8.96° and a 1.42 Å length for the central 4,4′-C−C. When these two species are associated with each other as the trisradical $CBPQT^{2(\bullet+)}\subset MV^{\bullet+}$ host−guest complex, the solid-state structure reveals that this bond length remains the same for the $CBPQT^{2(\bullet+)}$ component and increases slightly to 1.43 Å for the $MV^{\bullet+}$ radical cation. The torsional angles for both components continue to decrease to 0.38° and 0.07°, respectively. Accordingly, less change in terms of the antibonding character occur upon complexation of $MV^{\bullet+}$ with the $CBPQT^{2(\bullet+)}$ ring. This observation agrees with quantum mechanical calculations predicting that only a relatively small amount of charge is transferred[27] from the host to the guest. This insignificant change in the bond order is also reflected in the Raman spectroscopic behavior of the trisradical complex in solution as well as the solid state.

Raman Spectroscopy. The trisradical $CBPQT^{2(\bullet+)}\subset MV^{\bullet+}$ host−guest complex, as well as its free components, were investigated (Figure 5A) by solution-phase resonance Raman scattering spectroscopy in MeCN at 298 K. A solution of the free diradical dicationic $CBPQT^{2(\bullet+)}$ was subjected to laser irradiation at λ_{ex} = 532 nm, resulting in Raman spectroscopic resonances that were recorded in the region of 500−2000 cm^{-1}. In particular, the bands that are observed are significantly different from those of the fully oxidized $CBPQT^{4+}$ ring previously reported in the literature.[42−44] In addition to this difference, the $CBPQT^{2(\bullet+)}$ diradical dication

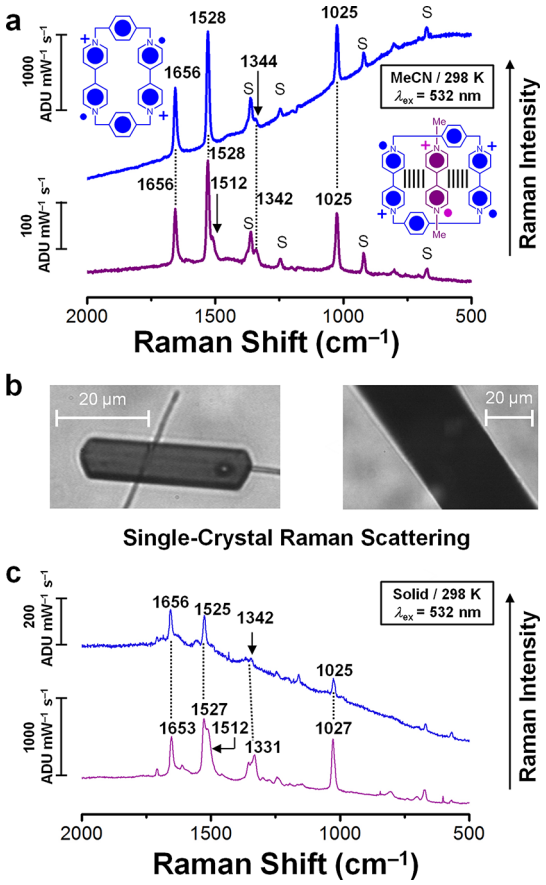

Figure 5. (a) Resonance Raman spectra of the free CBPQT$^{2(\bullet+)}$ ring (blue trace) and the trisradical CBPQT$^{2(\bullet+)}\subset$MV$^{\bullet+}$ complex (purple trace). Both spectra were recorded in MeCN at 298 K using 1.0 mM solutions. Note that the broad increase in intensity of the spectrum for CBPQT$^{2(\bullet+)}$ is a result of fluorescence emission. (b) Single crystals of CBPQT$^{2(\bullet+)}$ (left) and the trisradical complex CBPQT$^{2(\bullet+)}\subset$MV$^{\bullet+}$ (right) used in the single-crystal Raman scattering experiments shown in panel c. (c) Solid-state Raman spectroscopy of CBPQT$^{2(\bullet+)}$ (blue) and CBPQT$^{2(\bullet+)}\subset$MV$^{\bullet+}$ (purple) using a 532 nm laser at 298 K.

is slightly fluorescent at 532 nm and manifests as a broad band in the lower energy portion of the spectrum. Important to note here is the fact that the MV$^{\bullet+}$ radical cation was so fluorescent at λ_{ex} = 532 nm, that the (see Supporting Information) fluorescence obscured the observation of Raman scattering. When complexed with the CBPQT$^{2(\bullet+)}$ ring, however, the fluorescence of MV$^{\bullet+}$ is quenched. We hypothesize that the increased rigidity of the MV$^{\bullet+}$ is a consequence of the sp^2 character of the central 4,4′-C−C bond and leads to its fluorescent behavior. The same is true for the CBPQT$^{2(\bullet+)}$ diradical dication although, having more degrees of freedom, it is more readily quenched and the CBPQT$^{2(\bullet+)}\subset$MV$^{\bullet+}$ complex is totally quenched. The position and number of the peaks observed in the resonance Raman spectrum of the trisradical CBPQT$^{2(\bullet+)}\subset$MV$^{\bullet+}$ complex is nearly identical to those obtained for the free CBPQT$^{2(\bullet+)}$ diradical dication, the largest difference being the absence of the fluorescence emission band and a small shoulder appearing beside the 1528 cm^{-1} band at 1512 cm^{-1}. The Raman spectrum of the MV$^{\bullet+}$ radical cation in H_2O, previously reported,[45] shows peaks that are consistent with those observed for the CBPQT$^{2(\bullet+)}$ reported here. The fact that the positions of the Raman peaks undergo very little change on going from the free CBPQT$^{2(\bullet+)}$ diradical dication to the trisradical CBPQT$^{2(\bullet+)}\subset$MV$^{\bullet+}$ complex is consistent with the conclusions reached from X-ray structural analysis, further supporting the hypothesis that the bond order of the BIPY$^{\bullet+}$ radical cation components is conserved throughout complexation. The Raman spectra of MV$^{\bullet+}$ between its free and $(MV^{\bullet+})_2$ radical cation dimer have also been shown[46] to undergo little change as a consequence of dimerization other than the appearance of a similar shoulder band in the 1500 cm^{-1} region. These observations are in stark contrast to the Raman behavior previously reported[42] for the complex formed between the fully oxidized CBPQT^{4+} and neutral TTF, the spectra of which reveal significant changes in the energy of the vibrational modes of the CBPQT^{4+} ring upon complexation driven by π-donor−acceptor interactions.

Solid-state Raman spectroscopy recorded with an excitation wavelength of λ_{ex} = 532 nm was performed on single crystals (Figure 5B) of the free CBPQT$^{2(\bullet+)}$ host and the CBPQT$^{2(\bullet+)}\subset$MV$^{\bullet+}$ complex grown under similar conditions (see Experimental Methods) to those employed for the OFET device fabrication. First of all, the spectrum of the free CBPQT$^{2(\bullet+)}$ host reveals (Figure 5C) that the four most prominent Raman bands are observed at frequencies shifted only by a small amount (0−3 cm^{-1}) in comparison to the free CBPQT$^{2(\bullet+)}$ host studied in solution. The same observation is made when the solid-state spectrum of the CBPQT$^{2(\bullet+)}\subset$MV$^{\bullet+}$ complex is analyzed, namely, that the Raman spectrum remains relatively constant in both phases. A comparison of the solid-state Raman spectra observed for the free CBPQT$^{2(\bullet+)}$ host to the CBPQT$^{2(\bullet+)}\subset$MV$^{\bullet+}$ complex reveals that the two are almost identical in terms of the number of peaks and respective shifts. Just as in solution, a shoulder is observed at 1512 cm^{-1} in the spectrum of the CBPQT$^{2(\bullet+)}\subset$MV$^{\bullet+}$ complex that is absent in the spectrum of the free CBPQT$^{2(\bullet+)}$ host. Other than this shoulder, the other most significant difference between the two spectra are the relative intensities of the bands which are observed to change upon complexation. The similarities observed between the Raman spectra of the free host and the complex are a further indication that the bond order of the BIPY$^{\bullet+}$ radical cation components are not significantly changed after the transition to the solid state has occurred—a fact which is deeply connected with the ability of these crystals to serve as semiconducting materials in contrast to their mixed-stacked donor−acceptor redox relatives. These experimental results reflect the

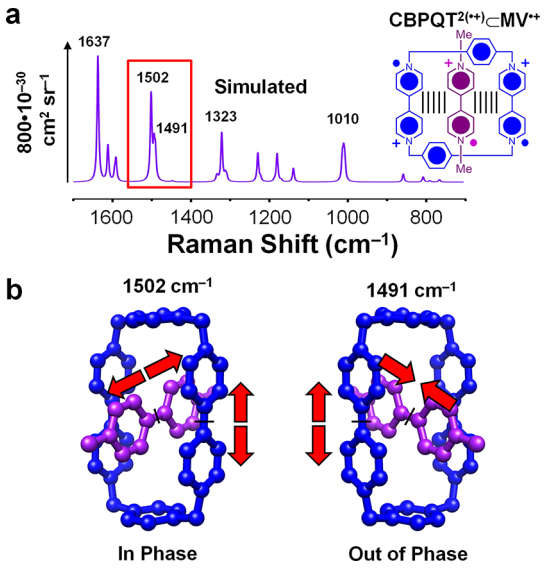

Figure 6. (a) Simulated Raman spectrum of CBPQT$^{2(\bullet+)}$⊂MV$^{\bullet+}$ using simulated Raman intensities of the neutral CBPQT⊂MV. Peaks are broadened by a Lorentzian with a full width at half-maximum of 10 cm^{-1}. (b) Graphical depictions of the vibrational modes that correspond to the calculated Raman bands observed at 1502 and 1491 cm^{-1}. The 1502 cm^{-1} band represents an in-phase stretching of the central 4,4′-C−C bonds of two of the interacting BIPY$^{\bullet+}$ units from host and guest, while the 1491 cm^{-1} band represents the out-of-phase stretch.

fact that complexation is not driven by donor−acceptor interactions as is the case for the CBPQT^{4+} ring with π-electron-rich guests, but by radical−radical interactions, a significant part of which comes from spin-pairing of the free radicals, and not by charge-donation. We hypothesize that the radical electron of the SOMO is smoothly distributed across the BIPY$^{\bullet+}$ radical cation components of the CBPQT$^{2(\bullet+)}$⊂MV$^{\bullet+}$ complex in the solid state, leading to the situation that contrasts with the electronically insulating behavior of single crystals of mixed stacks of donor−acceptor compounds and complexes.

To assign the Raman bands to specific vibrational modes of the trisradical CBPQT$^{2(\bullet+)}$⊂MV$^{\bullet+}$ complex, in particular the bands at 1528 and 1512 cm^{-1}, we carried out a series of quantum mechanical calculations. The Raman spectra of the open-shell MV$^{\bullet+}$, CBPQT$^{2(\bullet+)}$ and the CBPQT$^{2(\bullet+)}$⊂MV$^{\bullet+}$ complex were calculated using an approach (described in the Supporting Information) in which the Raman intensities of the related closed-shell forms were combined with the vibrational frequencies of the open-shell forms. This approach produced spectra that agreed well with the experimental data. The open-shell nature of the complex and its free components has little effect on the Raman intensities, instead, the greatest differences are in the frequencies of the vibrations themselves.

The calculated Raman spectrum of the trisradical CBPQT$^{2(\bullet+)}$⊂MV$^{\bullet+}$ complex is shown in Figure 6. The bands with calculated Raman shifts of 1502 and 1491 cm^{-1} correspond to those observed experimentally at 1528 and 1512 cm^{-1}, respectively, in solution. These bands are assigned to the vibrational motions involving both host and guest. The band at 1502 cm^{-1} involves an in-phase stretching of the central 4,4′-C−C bond of the BIPY$^{\bullet+}$ unit of the MV$^{\bullet+}$ guest coupled to the stretching of a BIPY$^{\bullet+}$ unit of the CBPQT$^{2(\bullet+)}$ host. The band at 1491 cm^{-1} represents a similar vibrational mode, except that the motion of the two BIPY$^{\bullet+}$ units occurs out of phase. The higher in-phase vibrational mode intensity is a consequence of the greater net change in polarizability accompanying changes in bond lengths that occur in-phase. These results lend further support to the notion that a minimal change in the bond order occurs upon complexation of the CBPQT$^{2(\bullet+)}$ host with the MV$^{\bullet+}$ guest, a fact which ultimately gives rise to its semiconductivity in the solid state.

CONCLUSIONS

Organic host−guest inclusion complexes driven by radical−radical interactions are relatively rare in comparison to the commonality of their donor−acceptor counterparts. Likewise, host−guest complexes which are conductive in the solid-state have yet to be widely explored as materials for electronic applications. In this article, we report the construction of an OFET using lithographic techniques, which apply source and drain leads to single crystals composed of a host−guest complex involving the diradical dicationic CBPQT$^{2(\bullet+)}$ ring complexed with the radical cationic MV$^{\bullet+}$ guest, and demonstrate their *p*-type semiconductivity. Resonance Raman spectroscopy and X-ray structural analyses reveal that the bond order of the BIPY$^{\bullet+}$ radical cationic subunits of each component changes very little upon complexation as well as after transitioning into the solid state as crystals. This constancy in bond order is related fundamentally to the fact that these trisradical complexes, by way of self-assembly, lead to conducting crystals in the solid-state. In contrast to mixed stacks of donor−acceptor complexes in their crystalline forms, which are known[47] for their electric *polarizability*, the minimal degree of charge-transfer associated with BIPY$^{\bullet+}$ radical−radical interactions provides a smooth "dipole-free" conduit for holes to flow in the valence band. Although the measured mobility[48] is over an order of magnitude less than best organic semiconductors reported, with the inherent modularity that host−guest chemistry carries with it, we envision being able to construct a suite of custom-made organic semiconducting materials, whose properties can be readily tuned by using a library of different organic radical cationic guests of varying electronic

and functional properties. This informed modular approach holds great promise as a design strategy for the large number of potential applications which employ these organic semiconductors as the active components in electronic materials and devices.

EXPERIMENTAL METHODS

All reagents were purchased from commercial suppliers (Aldrich or Fisher) and used without further purification. The $CBPQT\cdot 4PF_6$[38] and $MV\cdot 2PF_6$[25] were synthesized according to literature procedures. The purities of these compounds were determined by ^1H NMR spectroscopy supported by analytical HPLC monitored by UV−vis absorption. Reduction of $CBPQT^{4+}$ and MV^{2+} into the corresponding diradical dication $CBPQT^{2(\bullet+)}$ and radical cation $MV^{\bullet+}$ was achieved under nitrogen in the inert conditions provided by a glovebox in less than 1 h by vigorous stirring with activated zinc dust.

Crystal Growth. In a typical experiment, a solution of $CBPQT\cdot 4PF_6$ (0.63 mM) and $MV\cdot 2PF_6$ (0.75 mM) in degassed MeCN is stirred rigorously with an excess of zinc dust for 1 h. The zinc dust reduces both species to their radical cationic forms, namely $CBPQT^{2(\bullet+)}$ and $MV^{\bullet+}$. Following their reductions, complexation of the components ensues spontaneously, resulting in a dark purple solution. The zinc dust is then filtered off from the solution using a 0.45 μm syringe-tip filter. For the SEM and OFET experiments, the solution of the $CBPQT^{2(\bullet+)}\subset MV^{\bullet+}$ complex is layered onto a Si/SiO_2 wafer, and slow vapor diffusion of iPr_2O is allowed to proceed for approximately 5 days under the inert conditions of a glovebox. The yield of crystals composed of the $CBPQT^{2(\bullet+)}\subset MV^{\bullet+}$ complex, as opposed to their free host and guest components, was estimated to be quantitative by SEM; free $MV^{\bullet+}$ crystals, which were not observed, display a significantly different feather-like morphology. Crystals for solid-state Raman spectroscopy were grown by slow vapor diffusion of a solution of the $CBPQT^{2(\bullet+)}\subset MV^{\bullet+}$ into a vial for 5 days, after which time the crystals were transferred manually onto the surface of a glass slide.

OFET Device Fabrication and Characterization. The source−drain electrodes were fabricated using electron beam lithography. First of all, the SiO_2/Si substrates were spin-coated with MMA (8.5) MAA (6% concentration in ethyl lactate), baked at 180 °C for 1 min, then coated with PMMA (2% concentration in anisole). This was followed by baking at 180 °C for 1 min and exposure by a focused 30 keV electron beam in FEI Quanta FESEM. After development in MIBK/IPA 1:3 solution for 60 s, contact materials (Ti/Au, 3/100 nm thickness) were evaporated and lifted off in acetone. The heavily doped SiO_2/Si substrate was used as the back gate. Electrical characterization of OFET devices were carried out using a Keithley 4200 semiconductor characterization system with a shielded probe station with a micromanipulator in ambient air at room temperature.

Raman Spectroscopy. Resonance Raman spectroscopy was conducted in MeCN using an inverted microscope (Nikon Ti−U) equipped with a 50× objective (Nikon, Plan Fluor ELWD, numerical aperture of 0.55). The glass cell was epi-illuminated with continuous-wave laser light from Spectra Physics Millennia XV laser operating at 532 nm. Laser power (I_{ex}) was 61 μW at the sample, which we confirmed did not cause photodegradation of the sample. Scattered light was collected using the same objective, filtered for residual laser light (Semrock, Razoredge, long pass 532), and focused on the entrance slit of a $^1/_3$ m imaging spectrograph (SP2300, Princeton Instruments). The Raman light was dispersed using a 1200 groove/mm grating and collected on a LN2-cooled CCD (Spec10:400BR, Princeton Instruments). Experimental conditions: $\lambda_{ex} = 532$ nm, $I_{ex} = 61$ μW, acquisition time (t_{aq}) was 10 s. Solid-state Raman spectroscopy was conducted using the same experimental instrumentations except that the crystal samples were placed on a #1.5 coverslip (Warner Instruments).

Conflict of Interest: The authors declare no competing financial interest.

Acknowledgment. We acknowledge support from the World Class University (WCU) Program (R-31-2008-000-10055-0) in Korea and the Air Force Office of Scientific Research (AFOSR) under the Multidisciplinary Research Program of the University Research Initiative (MURI), Award FA9550-07-1-0534 entitled "Bioinspired Supramolecular Enzymatic Systems" in the United States. Dr. D. J. Late would like to thank Indo-US Science and technology forum (IUSSTF) for the award of postdoctoral fellowship, and Prof. C.N.R. Rao for support and encouragement. We also thank the National Science Foundation for the award of a Graduate Research Fellowship to A.C.F. J.C.B. acknowledges support from a National Defense Science and Engineering Graduate Fellowship. R.P.V.D. acknowledges support from the National Science Foundation Grant CHE-0911145. G.C.S. and N.V. acknowledge DOE BES Grant SC-0004752.

Supporting Information Available: Details of fluorescence emission spectroscopy and calculated Raman spectra. This material is available free of charge via the Internet at http://pubs.acs.org.

REFERENCES AND NOTES

1. Ratera, I.; Veciana, J. Playing with Organic Radicals as Building Blocks for Functional Molecular Materials. *Chem. Soc. Rev.* **2012**, *41*, 303–349.
2. Chiarelli, R.; Novak, M. A.; Rassat, A.; Tholence, J. L. A Ferromagnetic Transition at 1.48 K in an Organic Nitroxide. *Nature* **1993**, *363*, 147–149.
3. Green, J. E.; Choi, J. W.; Boukai, A.; Bunimovich, Y.; Johnston-Halperin, E.; Delonno, E.; Luo, Y.; Sheriff, B. A.; Xu, K.; Shin, Y. S.; *et al.* A 160-Kilobit Molecular Electronic Memory Patterned at 10^{11} Bits Per Square Centimetre. *Nature* **2007**, *445*, 414–417.
4. Lee, J.; Lee, E.; Kim, S.; Bang, G. S.; Shultz, D. A.; Schmidt, R. D.; Forbes, M. D. E.; Lee, H. Nitronyl Nitroxide Radicals as Organic Memory Elements with Both n- and p-Type Properties. *Angew. Chem., Int. Ed.* **2011**, *50*, 4414–4418.
5. Nakahara, K.; Oyaizu, K.; Nishide, H. Organic Radical Battery Approaching Practical Use. *Chem. Lett.* **2011**, *40*, 222–227.
6. Simon, P.; Gogotsi, Y. Materials for Electrochemical Capacitors. *Nat. Mater.* **2008**, *7*, 845–854.
7. Loser, S.; Bruns, C. J.; Miyauchi, H.; Ortiz, R. P.; Facchetti, A.; Stupp, S. I.; Marks, T. J. A Naphthodithiophene−Diketopyrrolopyrrole Donor Molecule for Efficient Solution-Processed Solar Cells. *J. Am. Chem. Soc.* **2011**, *133*, 8142–8145.
8. Bryce, M. R. Recent Progress on Conducting Organic Charge-Transfer Salts. *Chem. Soc. Rev.* **1991**, *20*, 355–390.
9. Jérome, D. The Physics of Organic Superconductors. *Science* **1991**, *252*, 1509–1514.
10. Geiser, U.; Schlueter, J. A. Conducting Organic Radical Cation Salts with Organic and Organometallic Anions. *Chem. Rev.* **2004**, *104*, 5203–5241.
11. Ferraris, J.; Cowan, D. O.; Walatka, V., Jr.; Perlstein, J. H. Electron-Transfer in a New Highly Conducting Donor−Acceptor Complex. *J. Am. Chem. Soc.* **1973**, *95*, 948–949.
12. Kosower, E. M.; Hajdu, J. Pyridinyl Diradical π-Mer. Magnesium Iodide Complexes. *J. Am. Chem. Soc.* **1971**, *93*, 2534–2535.
13. Geuder, W.; Hünig, S.; Suchy, A. Single and Double Bridged Viologenes and Intramolecular Pimerization of Their Cation Radicals. *Tetrahedron* **1986**, *42*, 1665–1677.
14. Pal, S. K.; Bag, P.; Sarkar, A.; Chi, X.; Itkis, M. E.; Tham, F. S.; Donnadieu, B.; Haddon, R. C. Hysteretic Spin and Charge Delocalization in a Phenalenyl-Based Molecular Conductor. *J. Am. Chem. Soc.* **2010**, *132*, 17258–17264.
15. Ziganshina, A. Y.; Ko, Y. H.; Jeon, W. S.; Kim, K. Stable π-Dimer of a Tetrathiafulvalene Cation Radical Encapsulated in the Cavity of Cucurbit[8]Uril. *Chem. Commun.* **2004**, 806–807.

16. Yoshizawa, M.; Kumazawa, K.; Fujita, M. Room-Temperature and Solution-State Observation of the Mixed-Valence Cation Radical Dimer of Tetrathiafulvalene, $[(TTF)_2]^{+\bullet}$, within a Self-Assembled Cage. *J. Am. Chem. Soc.* **2005**, *127*, 13456–13457.
17. Spruell, J. M.; Coskun, A.; Friedman, D. C.; Forgan, R. S.; Sarjeant, A. A.; Trabolsi, A.; Fahrenbach, A. C.; Barin, G.; Paxton, W. F.; Dey, S. K.; *et al.* Highly Stable Tetrathiafulvalene Radical Dimers in [3]Catenanes. *Nat. Chem.* **2010**, *2*, 870–879.
18. Coskun, A.; Spruell, J. M.; Barin, G.; Fahrenbach, A. C.; Forgan, R. S.; Colvin, M. T.; Carmieli, R.; Benítez, D.; Tkatchouk, E.; Friedman, D. C.; *et al*. Mechanically Stabilized Tetrathiafulvalene Radical Dimers. *J. Am. Chem. Soc.* **2011**, *133*, 4538–4547.
19. Becher, J.; Lau, J.; Mork, P. Oligotetrathiafulvalenes. In *Electronic Materials: The Oligomer Approach*; Müllen, K., Wegner, G., Eds.; Wiley-VCH: Weinheim Germany, 1998; pp 198−233.
20. Saito, G.; Yamochi, H.; Maesato, M.; Yoshida, Y.; Ota, A.; Shimizu, Y. Design of Organic (Super)Conductors and Study of their Physical Properties. In *Organic Conductors, Superconductors, and Magnets: From Synthesis to Molecular Electronics*; Ouahab, L., Yagubskii, , E., Eds.; Kluwer Academic Publishers: New York, 2004; pp 19−44.
21. Michaelis, L.; Hill, E. S. The Viologen Indicators. *J. Gen. Physiol.* **1933**, *16*, 859–873.
22. Michaelis, L. Semiquinones, the Intermediate Steps of Reversible Organic Oxidation−Reduction. *Chem. Rev.* **1935**, *16*, 243–286.
23. Kosower, E. M.; Cotter, J. L. Stable Free Radicals. II. The Reduction of 1-Methyl-4-cyanopyridinium Ion to Methylviologen Cation Radical. *J. Am. Chem. Soc.* **1964**, *86*, 5524–5527.
24. Bird, C. L.; Kuhn, A. T. Electrochemistry of the Viologens. *Chem. Soc. Rev.* **1981**, *10*, 49–82.
25. Monk, P. M. S. The Radical Cation: Dimer Formation. In *The Viologens: Physicochemical Properties, Synthesis, and Applications of the Salts of 4,4′-Bipyridine*; Wiley: New York, 1998; pp 115−131.
26. Bockman, T. M.; Kochi, J. K. Isolation and Oxidation-Reduction of Methylviologen Cation Radicals. Novel Disproportionation in Charge-Transfer Salts by X-ray Crystallography. *J. Org. Chem.* **1990**, *55*, 4127–4135.
27. Trabolsi, A.; Khashab, N.; Fahrenbach, A. C.; Friedman, D. C.; Colvin, M. T.; Cotí, K. K.; Benítez, D.; Tkatchouk, E.; Olsen, J.-C.; Belowich, M. E.; *et al*. Radically Enhanced Molecular Recognition. *Nat. Chem.* **2010**, *2*, 42–49.
28. Fahrenbach, A. C.; Barnes, J. C.; Lanfranchi, D. A.; Li, H.; Coskun, A.; Gassensmith, J. J.; Liu, Z.; Benítez, D.; Trabolsi, A.; Goddard, W. A., III; *et al.* Solution-Phase Mechanistic Study and Solid-State Structure of a Tris(bipyridinium radical cation) Inclusion Complex. *J. Am. Chem. Soc.* **2012**, *134*, 3061–3072.
29. Li, H.; Fahrenbach, A. C.; Dey, S. K.; Basu, S.; Trabolsi, A.; Zhu, Z.; Botros, Y. Y.; Stoddart, J. F. Mechanical Bond Formation by Radical Templation. *Angew. Chem., Int. Ed.* **2010**, *49*, 8260–8265.
30. Stoddart, J. F. The Chemistry of the Mechanical Bond. *Chem. Soc. Rev.* **2009**, *38*, 1802–1820.
31. Li, H.; Fahrenbach, A. C.; Coskun, A.; Zhu, Z.; Barin, G.; Zhao, Y.-L.; Botros, Y. Y.; Sauvage, J.-P.; Stoddart, J. F. A Light-Stimulated Molecular Switch Driven by Radical−Radical Interactions in Water. *Angew. Chem., Int. Ed.* **2011**, *50*, 6782–6788.
32. Deng, H.; Olson, M. A.; Stoddart, J. F.; Yaghi, O. M. Robust Dynamics. *Nat. Chem.* **2010**, *2*, 439–443.
33. Sze, S. M.; Ng, K. K. MOSFETs. In *Physics of Semiconductor Devices*; 3rd ed.; Wiley-Interscience: Hoboken, N.J., 2007; pp 293−373.
34. Lü, J.-M.; Rosokha, S. V.; Kochi, J. K. Stable (Long-Bonded) Dimers *via* the Quantitative Self-Association of Different Cationic, Anionic, and Uncharged π-Radicals: Structures, Energetics, and Optical Transitions. *J. Am. Chem. Soc.* **2003**, *125*, 12161–12171.
35. Sun, D.-L.; Rosokha, S. V.; Lindeman, S. V.; Kochi, J. K. Intervalence (Charge-Resonance) Transitions in Organic Mixed-Valence Systems. Through-Space *versus* through-Bond Electron Transfer between Bridged Aromatic (Redox) Centers. *J. Am. Chem. Soc.* **2003**, *125*, 15950–15963.
36. Odell, B.; Reddington, M. V.; Slawin, A. M. Z.; Spencer, N.; Stoddart, J. F.; Williams, D. J. Cyclobis(Paraquat-*p*-phenylene)—A Tetracationic Multipurpose Receptor. *Angew. Chem., Int. Ed.* **1988**, *27*, 1547–1550.
37. Asakawa, M.; Dehaen, W.; L'abbé, G.; Menzer, S.; Nouwen, J.; Raymo, F. M.; Stoddart, J. F.; Williams, D. J. Improved Template-Directed Synthesis of Cyclobis(Paraquat-*p*-phenylene). *J. Org. Chem.* **1996**, *61*, 9591–9595.
38. Sue, C.-H.; Basu, S.; Fahrenbach, A. C.; Shveyd, A. K.; Dey, S. K.; Botros, Y. Y.; Stoddart, J. F. Enabling Tetracationic Cyclophane Production by Trading Templates. *Chem. Sci.* **2010**, *1*, 119–125.
39. Philp, D.; Slawin, A. M. Z.; Spencer, N.; Stoddart, J. F.; Williams, D. J. The Complexation of Tetrathiafulvalene by Cyclobis(Paraquat-*p*-phenylene). *J. Chem. Soc., Chem. Commun.* **1991**, 1584–1586.
40. Asakawa, M.; Ashton, P. R.; Balzani, V.; Credi, A.; Hamers, C.; Mattersteig, G.; Montalti, M.; Shipway, A. N.; Spencer, N.; Stoddart, J. F.; *et al.* A Chemically and Electrochemically Switchable [2]Catenane Incorporating a Tetrathiafulvalene Unit. *Angew. Chem., Int. Ed.* **1998**, *37*, 333–337.
41. Benítez, D.; Tkatchouk, E.; Yoon, I.; Stoddart, J. F.; Goddard, W. A., III. Experimentally-Based Recommendations of Density Functionals for Predicting Properties in Mechanically Interlocked Molecules. *J. Am. Chem. Soc.* **2008**, *130*, 14928–14929.
42. Witlicki, E. H.; Hansen, S. W.; Christensen, M.; Hansen, T. S.; Nygaard, S. D.; Jeppesen, J. O.; Wong, E. W.; Jensen, L.; Flood, A. H. Determination of Binding Strengths of a Host−Guest Complex Using Resonance Raman Scattering. *J. Phys. Chem. A* **2009**, *113*, 9450–9457.
43. Witlicki, E. H.; Andersen, S. S.; Hansen, S. W.; Jeppesen, J. O.; Wong, E. W.; Jensen, L.; Flood, A. H. Turning on Resonant SERRS Using the Chromophore-Plasmon Coupling Created by Host−Guest Complexation at a Plasmonic Nanoarray. *J. Am. Chem. Soc.* **2010**, *132*, 6099–6107.
44. Witlicki, E. H.; Johnsen, C.; Hansen, S. W.; Silverstein, D. W.; Bottomley, V. J.; Jeppesen, J. O.; Wong, E. W.; Jensen, L.; Flood, A. H. Molecular Logic Gates Using Surface-Enhanced Raman-Scattered Light. *J. Am. Chem. Soc.* **2011**, *133*, 7288–7291.
45. Poizat, O.; Sourisseau, C.; Corset, J. Vibrational and Electronic Study of the Methyl Viologen Radical Cation MV^+ in the Solid-State. *J. Mol. Struct.* **1986**, *143*, 203–206.
46. Forster, M.; Girling, R. B.; Hester, R. E. Infrared, Raman and Resonance Raman Investigations of Methylviologen and Its Radical Cation. *J. Raman. Spectrosc.* **1982**, *12*, 36–48.
47. Tayi, A. S.; Shveyd, A. K.; Sue, A. C.-H.; Szarko, J. M.; Rolczynski, B. S.; Cao, D.; Kennedy, T. J.; Sarjeant, A. A.; Stern, C. L.; Paxton, W. F.; *et al.* Room-Temperature Ferroelectricity in Supramolecular Networks of Charge-Transfer Complexes. *Nature* **2012**, *488*, 485–489.
48. Wang, C.; Dong, H.; Hu, W.; Liu, Y.; Zhu, D. Semiconducting π-Conjugated Systems in Field-Effect Transistors: A Material Odyssey of Organic Electronics. *Chem. Rev.* **2012**, *112*, 2208–2267.